Chemical Science

ROYAL SOCIETY OF CHEMISTRY

EDGE ARTICLE

View Article Online
View Journal | View Issue

Cite this: *Chem. Sci.*, 2025, **16**, 7971

All publication charges for this article have been paid for by the Royal Society of Chemistry

A novel boron-stereogenic fluorophore with dual-state circular polarization luminescence *via* a self-dispersing strategy†

Changjiang Yu, *[a] Chao Cheng,[a] Zhangzhan Liu,[b] Zhigang Ni, [c] Zujin Zhao,*[b] Hua Lu, *[c] Erhong Hao *[a] and Lijuan Jiao *[a]

Molecular engineering is a reliable approach for the development of circularly polarized luminescence (CPL) materials for various applications. However, creating dual-state CPL platforms that possess chirality while achieving a delicate balance between molecular rigidity and flexibility remains a formidable challenge. In this study, a novel bisarylboron-anchored pyrrolylsalicylhydrazone (BOPSH) platform was synthesized *via* a facile "one-pot" condensation. These key aryl-boron substituents not only provide structural rigidity to the fluorophore, enhancing the bright emission and suppressing emission quenching from π–π stacking in solid states due to their twisting and bulky steric effects, but also generate a boron-stereogenic center and enable strong CPL by promoting intramolecular charge-transfer transitions. As a result, these BOPSHs show intense absorption and strong dual-state emissions in both solution and solid states (with Φ_{PL} value approaching unity), emitting across the visible region with excellent chemical, photostability, and thermal stability. Meanwhile, their enantiomers display dual-state CPL performance, with luminescence dissymmetry factors (g_{lum}) up to 9.40 × 10^{-3}, and CP electroluminescence (EL) with a dissymmetry factor (g_{EL}) of 3.07 × 10^{-3}, along with excellent maximum external quantum efficiencies ($\eta_{ext,max}$) of 5.0%, approaching the theoretical limit for fluorescent molecules. We expect our study to break new ground in the construction of chiral dual-state materials with diverse structures.

Received 9th February 2025
Accepted 27th March 2025

DOI: 10.1039/d5sc01025j

rsc.li/chemical-science

Introduction

A fundamental characteristic of symmetry is chirality; chiral molecules and other chiral objects exist as pairs of non-superimposable mirror images.[1] In molecular design, chirality is typically considered for various applications, including life sciences, biomedicine, and materials science.[2] Utilizing the polarization of photons and the spin of electrons, chirality offers a novel approach to achieving circular polarization luminescence (CPL) for various applications, including 3D displays, encrypted optical communication, and bioimaging.[3,4]

Early research on CPL materials focused on lanthanide or transition metal-based complexes, which have high dissymmetry factors but often suffer from low molar absorption coefficients (ε) and fluorescence quantum yields (Φ_{PL}) due to the Laporte-forbidden rule.[5] In contrast, chiral organic small molecules offer several advantages, including large ε, higher emission efficiency, easier chemical structure modification, precise emission wavelength tuning, and simpler fabrication.[6] As a result, CPL-active organic small molecules have garnered increasing attention.[7] However, most of these molecules contain polycyclic aromatic structures, which tend to form strong π–π stacking in concentrated solutions or solid states.[8] This results in aggregation-caused quenching (ACQ), leading to weak or negligible CPL emission, which hinders their use in applications requiring highly emissive solid-state compounds, such as OLEDs or light-emitting electrochemical cells.[9]

A promising alternative is the development of chiral aggregation-induced emission (AIE) fluorophores, which can emit CPL in aggregated states.[10] However, a limitation of these fluorophores is their lack of emission in solution due to fast molecular motions and vibrations, which suppress fluorescence. This raises a key challenge in designing dual-state emissive (DSE) chiral molecules: achieving chirality while maintaining a delicate balance between molecular conformational freedom, which prevents fluorescence quenching in the

[a]*Key Laboratory of Functional Molecular Solids, Ministry of Education, School of Chemistry and Materials Science, Anhui Normal University, Wuhu, 241002, China. E-mail: yuchj@ahnu.edu.cn; haoehong@ahnu.edu.cn; jiao421@ahnu.edu.cn*

[b]*State Key Laboratory of Luminescent Materials and Devices, Guangdong Provincial Key Laboratory of Luminescence from Molecular Aggregates, South China University of Technology, Guangzhou, 510640, China. E-mail: mszjzhao@scut.edu.cn*

[c]*Key Laboratory of Organosilicon Chemistry and Material Technology, Ministry of Education, Zhejiang Key Laboratory of Organosilicon Material Technology, College of Material Chemistry and Chemical Engineering, Hangzhou Normal University, Hangzhou, 311121, Zhejiang, China. E-mail: hualu@hznu.edu.cn*

† Electronic supplementary information (ESI) available: Experimental details, NMR, HRMS, photophysical, electrochemical, theoretical data, chiroptical data, and additional supplementary figures. CCDC 2116412, 2389168, 2116411, 2116409, 2116410, 2251717 and 2251718. For ESI and crystallographic data in CIF or other electronic format see DOI: https://doi.org/10.1039/d5sc01025j

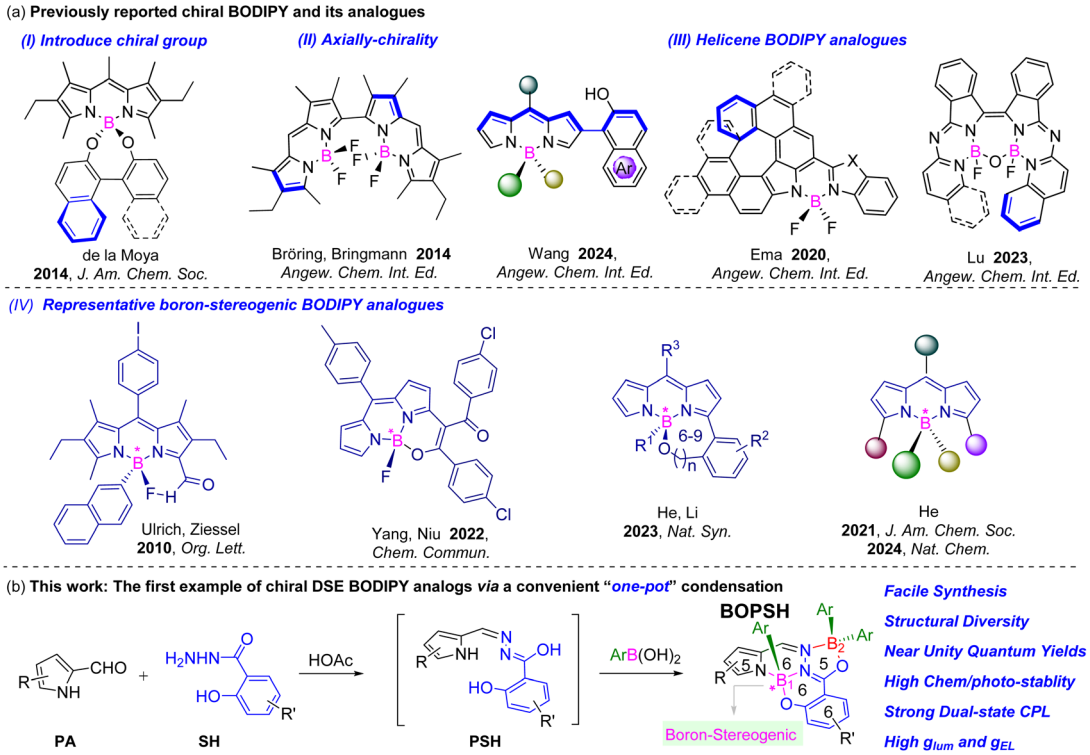

Fig. 1 (a) Previously reported chiral BODIPY and its analogues. (b) The chiral DSE BOPSH fluorophore designed in this work.

solid state, and minimizing nonradiative relaxation in solution to ensure strong emission.[11]

The boron dipyrromethene (BODIPY) chromophore is an attractive platform for constructing organic CPL molecules due to its rich chemistry and tuneable optical and electronic properties, such as intense visible absorption, fluorescence brightness, and good photostability.[12,13] A series of chiral BODIPY derivatives (Fig. 1a) have been reported by incorporating chiral moieties from the periphery, augmenting scaffolds with chiral axes, and integrating helicene units.[14–17] Very recently, several catalytic synthesis methods have been developed for the boron-stereogenic chiral BODIPYs through the desymmetrization reactions of prochiral tetracoordinated boron substrates.[16b,18,19] However, these compounds have failed to demonstrate CPL in the solid state. The rational design of chiral DSE BODIPYs and their analogues as luminescent materials remains a significant challenge that has yet to be addressed. Therefore, there is an urgent need to explore novel chiral DSE BODIPY systems with tuneable CPL for both fundamental research and practical applications.

By analyzing the core of the BODIPY chromophore, which generally assembles *via* BF_2 complexation of an *N*,*N*-bidentate dipyrromethene ligand, we propose the preparation of a suitable ligand of pyrrolylsalicylhydrazone featuring two independent boron coordination sites (*N*,*N*,*O*-tridentate coordination site for B1 and *N*,*O*-bidentate coordination site for B2, Fig. 1b). This ligand, when subjected to direct electrophilic aryl-boron substitutions, is expected to yield a novel bis-boron-chelated fluorophore with the desired structure rigidity and essential steric hindrances to promote successful self-dispersion of the fluorophore, ensuring strong DSE performance. Additionally, the aryl-boron substituents on the *N*,*N*,*O*-tridentate coordination B1 site will also generate a boron-stereogenic center *in situ*. Moreover, these aryl-boron substituents may facilitate intramolecular charge-transfer (ICT) transitions due to their electron deficiency, resulting in enhanced CPL luminescence.[20] Based on this reasoning, we design a self-dispersing triarylboron-anchored pyrrolylsalicylhydrazone (BOPSH) fluorophore featuring two independent boron coordination sites. This can be directly accessed *via* "one-pot" electrophilic aryl-boron substitutions on the pyrrolylsalicyhydrazone ligand by condensing the readily accessible 2-formylpyrrole with salicylhydrazines, followed by subsequent *in situ* complexation with commercial arylboronic acids. Expectedly, they exhibit DSE emission (Φ_{PL} value approaching unity) across the visible region. Additionally, these configurationally stable enantiomers display good solid-state CPL and CP electroluminescence (CPEL) with corresponding dissymmetry factors up to 9.40×10^{-3} and 3.07×10^{-3}, respectively.

Results and discussion

Syntheses and characterization

The synthesis involves a condensation reaction between readily available formylpyrrole/isoindole and salicylhydrazine, followed by on-site complexation with commercial arylboronic acids. The condensation of 2-formylpyrrole with salicylhydrazine in the presence of a catalytic amount of glacial acetic acid (HOAc, Scheme 1a) and subsequent complexation with phenylboronic acid generated two products. Among those, the

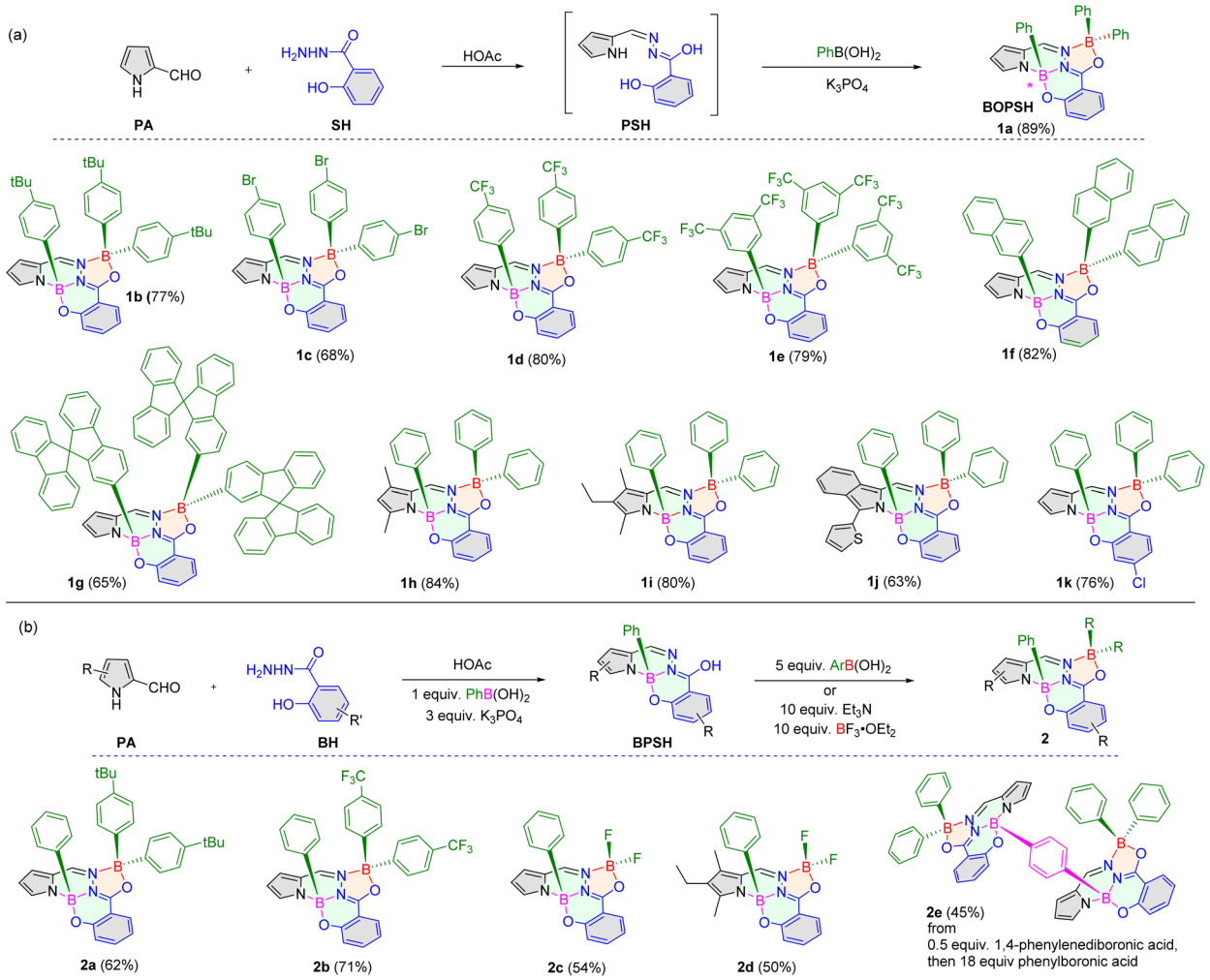

Scheme 1 Syntheses of BOPSHs **1a–k** and **2a–e**.

weakly fluorescent product was characterized as a mono-boron coordinated compound, while the bright fluorescent one, confirmed *via* X-ray analysis was a bisboron-anchored BOPSH **1a** (Scheme 1a). Following further optimization of the reaction conditions by screening solvents, temperature, base, and reagent ratios, BOPSH **1a** was ultimately obtained as the sole product in an 89% isolated yield.

To enrich structural diversity, various commercial arylboronic acids were applied in this reaction, successfully yielding the desired BOPSHs **1b–g** in 65–82% yields (Scheme 1a). We further extended this optimized reaction condition to the condensation of 2-formylpyrrole/isoindole derivatives with salicylhydrazide. After subsequent complexation with phenylboronic acid, BOPSHs **1h–j** were generated in 63–84% yields. Additionally, the one-pot condensation of 4-chloro-2-hydroxybenzohydrazide and 2-formylpyrrole, followed by phenylboronic acid also provided BOPSH **1k** in 76% yield.

We found that the boron complexations occurred in a stepwise fashion. By reducing the ratio of phenylboronic acid to one equivalent, no formation of BOPSH **1a** was obtained and only mono-boron coordinated BPSH was obtained (Scheme 1b). This indicates that the boron complexation selectively first took place with the nitrogen of pyrrole and the oxygen of the phenol moiety, forming a four-aromatic-ring-fused BPSH structure. This provided us the opportunity to install two different aryl moieties onto the boron atoms of the BOPSH chromophore to achieve BOPSHs **2a** and **2b** (Scheme 1b) *via* further complexation of BPSH with 4-*tert*-butyl and 4-trifluoromethyl-substituted phenylboronic acids. Similarly, BOPSHs **2c** and **2d** were prepared using $BF_3 \cdot OEt_2$ to coordinate with the second unilateral boron site, achieving yields of 54% and 50%, respectively. Through the complexation of BPSH with *p*-phenyl-1,4-diboronic acid, a face-to-face four-boron coordinated dimeric BOPSH **2e** was also isolated in a 45% yield (Scheme 1b). These novel BOPSHs were fully characterized using ^{1}H, ^{13}C, ^{11}B NMR, and HRMS.

X-ray crystal structure analysis

To confirm the boron-stereogenic center architecture, single crystals of racemic BOPSHs **1a**, **1e**, and **1h–k**, as well as **2e**, suitable for X-ray analysis were obtained by the slow diffusion of hexane into their dichloromethane solutions (Tables S1–S4†).

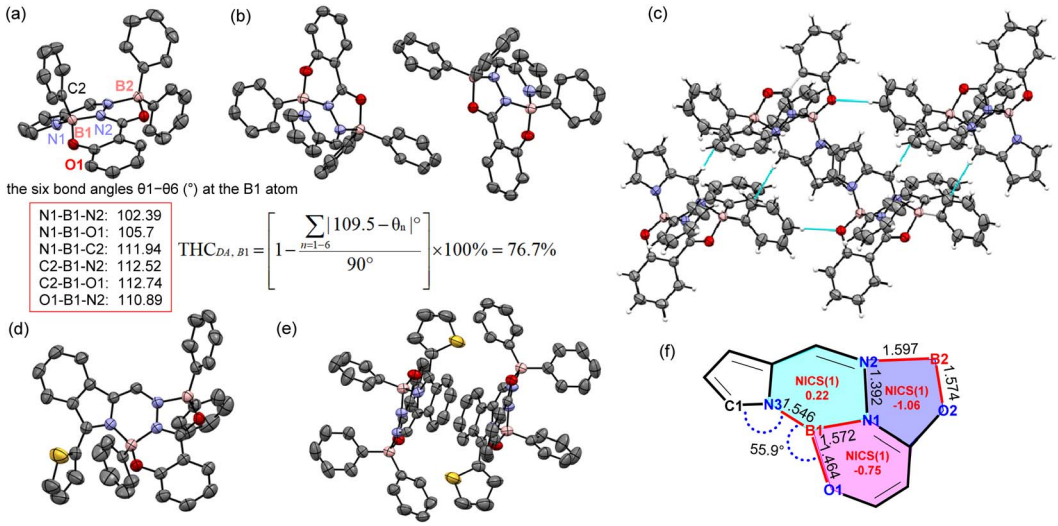

Fig. 2 (a)–(c) X-ray crystal, dimmer, and packing structures of **1a**. (d) and (e) X-ray crystal and dimer structures of **1j**. (f) NICS(1) values for **1a**. Peripheral substituents and hydrogen atoms were removed for clarity. Thermal ellipsoids are shown at the 50% probability level. Selected bond lengths in **1a**: B1–N1, 1.572 Å; B1–N3, 1.545 Å; B2–N2, 1.597 Å; B1–O1, 1.464 Å; B2–O2, 1.574 Å. C, gray; N, light blue; B, pink; O, red; S, yellow.

As shown in Fig. 2 and S1–S7,† the rigid heteroatom BOPSH core consists of five fused aromatic rings, including one pyrrole, one phenyl, one newly formed five-membered ring, and two newly formed six-membered rings. The dihedral angle between C1–N3–B1 and O1–N3–B1 is 55.9°, and the half-bowl conformation, characterized by a large torsional angle (23.5° for **1a** and 32.2° for **1j**) between the aromatic groups on both sides of the B1 atom, indicates that the BOPSH core is distorted.

The bowls display a relatively shallow depth; for example, the bowl depth for **1a** is 1.24(3) Å. The B–O and B–N bond lengths in the five-membered ring (around 1.57(2) and 1.61(2) Å) are longer than those observed in the six-membered ring (1.47(2) and 1.56(2) Å). The tetrahedral character (THC_{DA}) of the B1 and B2 atoms in **1a** was calculated as 76.7% and 68.5%, respectively, according to Höpfl's equation,[21] based on the account of the six bond angles of the boron-related bonds, as shown in Fig. 2a and S8.† The packing structures of **1a** reveal two enantiomers without π–π stacking, and multiple C–H···π interactions (*ca.* 2.8 Å, Fig. 2c) are observed. The nucleus-independent chemical shift (1) (NICS(1)) values, calculated using density functional theory (DFT), for the B-containing rings, fall within the −1.06 to 0.22 ppm range, indicating a non-aromatic character.

Spectroscopic properties

These BOPSHs exhibit broad absorption and ultra-bright emission (Fig. 3, S9–S24, Tables 1 and S5–S7†). They absorb light with high molar extinction coefficients (ε_{max} up to 21 900 M^{-1} cm^{-1}) and emit light with Φ_{PL} of up to 97%. These results show that luminous intensity and spectral wavelength can be tuned through minor structural modifications. Importantly, they exhibit high brightness (up to 19 400 M^{-1} cm^{-1}). In comparison to common BODIPY dyes,[12,13] these BOPSHs demonstrate relatively larger Stokes shifts (2100–4500 cm^{-1}, Tables S5 and S6†) and longer fluorescence lifetimes (6.16–8.07 ns).

As demonstrated by **1a**, these newly developed BOPSHs show excellent stability in commonly used organic solvents. For example, no aggregation was observed with the increasing concentration of **1a** in toluene (from 2 μM to 40 μM), as indicated by the good linear correlation between the absorbance maxima and the concentrations of the solution (Fig. S25†). Negligible variations in absorbance were observed with changes in pH values in 1% acetonitrile PBS. Additionally, they exhibit excellent photostability in toluene, superior to that of fluorescein under the same light irradiation conditions. For instance, after 40 min of light irradiation using a 50 W LED lamp with an irradiance light dose of 84 J cm^{-2}, no detectable decrease in absorbance was observed for **1a**, while an approximate 60% decrease in absorbance was noted for fluorescein (Fig. S26†). Furthermore, the respective BOPSH dyes demonstrate excellent thermal stability, with a thermal decomposition temperature of 326 °C for **1a** and 278 °C for **1d**, as evidenced by thermogravimetric analysis (Fig. S27†).

BOPSHs **1a–k** and **2a–c** show very bright solid-state fluorescence (solid-state Φ_{PL} up to 89%, Table 1, Fig. 3a and S28–S38†) and can be easily tuned *via* simple variations of substituents. For example, BOPSH **1a** emits bright green light with a wavelength maximum of at 489 nm, with an absolute Φ_{PL} of 80%. The emission spectra are red-shifted to 532 nm for **1i** (Φ_{PL} = 56%, yellow light) and 622 nm for **1j** (Φ_{PL} = 21%, red light) in the powder states (Tables 1 and S7†). Additionally, the solid-state fluorescence emission spectra of these BOPSHs span from the sky-blue, green, and yellow regions to the red region (Fig. 3a). Most of their solid-state fluorescence lifetimes fall between 3.58 and 11.33 ns (Table 1). The long solid-state lifetimes for **1b** and **1e** (11.33 ns and 8.42 ns) may be attributed to the bulky substituents on the boron atom, which enhance the stability of the excited state and consequently prolong the fluorescence lifetime. It is worth noting that the absolute solid Φ_{PL} of **2c** and **2d** decreased, possibly due to the reduced steric

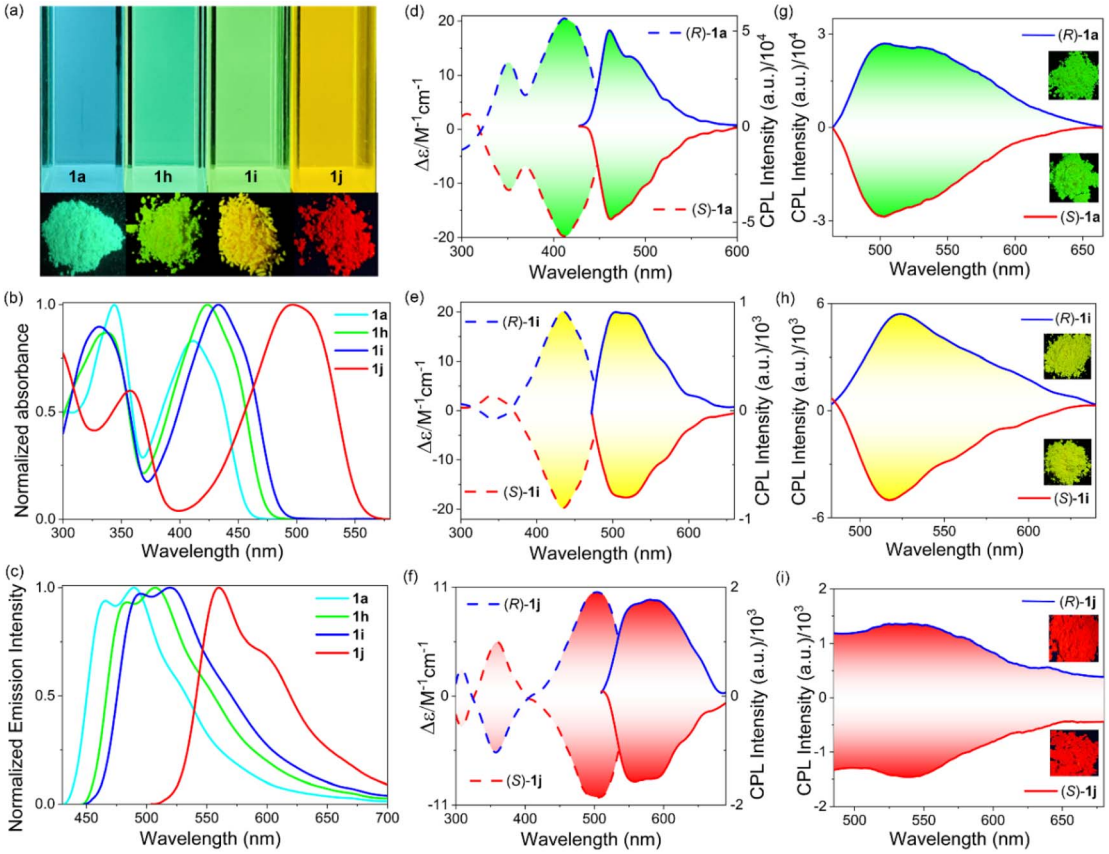

Fig. 3 Photophysical and chiroptical properties of **1a** and **1h–j** in dichloromethane and solid states. (a) Fluorescence photos of respective **1a** and **1h–j** taken under a 365 nm lamp. (b) Normalized UV-vis absorption and (c) emission spectra in dichloromethane. (d)–(f) CD (dash lines) and CPL spectra (solid lines) of (S/R)-**1a** (d) and (g), **1i** (e) and (h), and **1j** (f) and (i) in dichloromethane and solid states.

Table 1 Photophysical data of BOPSHs **1a–k** and **2a–e**

	Dichloromethane		Solid powder
Dyes	$\lambda_{abs}^{max a}$ (nm) (10^{-4} ε^{b})	$\lambda_{em}^{max a}$ (nm) (Φ^{c}, τ^{d} (ns))	λ_{em}^{max} (nm) (Φ^{c}, τ^{d} (ns))
1a	349 (4.15), 412 (4.08)	464, 489 (90%, 7.12)	489 (80%, 5.47)
1b	347 (3.99), 411 (3.92)	465, 492 (73%, 7.12)	501 (82%, 11.33)
1c	347 (4.13), 412 (4.05)	460, 489 (81%, 7.09)	492 (80%, 6.21)
1d	350 (4.16), 412 (4.09)	462, 488 (77%, 6.79)	513 (65%, 6.21)
1e	351 (4.08), 413 (3.92)	460, 486 (75%, 6.25)	492 (78%, 8.42)
1f	348 (4.16), 411 (4.09)	467, 489 (90%, 8.07)	494 (47%, 4.57)
1g	342 (4.14), 412 (3.97)	466, 489 (75%, 7.70)	493 (60%, 5.03)
1h	338 (4.17), 424 (4.23)	483, 507 (96%, 7.09)	523 (59%, 4.74)
1i	332 (4.16), 433 (4.21)	495, 521 (97%, 6.98)	532 (56%, 4.37)
1j	357 (4.07), 494 (4.29)	560 (77%, 6.16)	602 (21%, 3.71)
1k	358 (4.06), 420 (4.06)	474, 502 (65%, 6.79)	528 (89%, 6.76)
2a	347 (3.98), 411 (3.90)	463, 487 (79%, 7.28)	492 (45%, 5.14)
2b	349 (4.19), 412 (4.11)	463, 490 (77%, 6.87)	503 (37%, 3.58)
2c	348 (4.04), 416 (4.01)	468, 490 (59%, 5.57)	492 (15%, 3.89)
2d	337 (4.18), 428 (4.23)	476, 506 (62%, 5.69)	503 (17%, 1.83)
2e	346 (4.41), 412 (4.34)	465, 491 (78%, 7.60)	526 (81%, 4.61)

[a] Data correspond to the strongest absorption or emission wavelength maxima. [b] Molar extinction coefficient (ε) in M^{-1} cm^{-1}. [c] Absolute fluorescence quantum yields. [d] Fluorescence lifetime.

hindrance of the BF_2 unit. Compared to the non-fluorescent mono-boron BPSH, the structural rigidity of BOPSHs enhanced by dual boron coordination significantly improves their bright emissions in solutions and solid states. The results reveal that the two phenyl rings of the BPh_2 group are essential for enhancing the solid-state fluorescence of these BOPSH dyes.

Additionally, no obvious intermolecular π–π stacking between these BOPSHs from adjacent molecules is observed. This is reflected in the increased π–π distance (ranging from 6.35 to 10.32 Å) and the lower degree of π–π overlap, which is similar to the recently developed AIE-type 1,4-bis(diphenylamino)-2,5-disubstituted benzene fluorophores exhibiting high solid-state fluorescence efficiency reported by Tang's group.[22] Additionally, they generally exhibit coplanar, inclined "staircase-like" arrangements with pitch angles ranging from 20.3° to 50.1° along the long molecular axis (Fig. S1–S7†), contributing to the enhanced solid-state Φ_{PL} for these BOPSHs. This is in good accordance with Kasha's exciton model.[23]

Interestingly, upon gentle grinding of crystalline **1a** with a spatula, a 28 nm blue shift (from 512 to 484 nm) was observed in the solid-state emission spectra, accompanied by an increased solid Φ_{PL} (Fig. S39a and Table S7†). Upon heating the ground powder, the fluorescence emission band reverted to 489 nm with a decreased Φ_{PL}. Similar results were also observed for **1i** (Fig. S39b and Table S7†). This red shift may be closely associated with a conformational change from a flat plate conformation in the crystalline state to a folded conformation upon grinding, as indicated by the X-ray powder diffraction analysis results. Sharp diffraction peaks were observed for these molecules in the crystalline state, demonstrating a highly ordered molecular arrangement. Upon grinding, some of these peaks (for example, signals a–c, Fig. S39c and d†) decreased in intensity or disappeared, suggesting a transition from a crystalline to an amorphous packing arrangement.

Electrochemical properties

Electrochemical properties were studied using cyclic voltammetry. Respective **1a**, **1i**, and **1j** displayed reversible one-electron oxidation and reduction processes (Fig. S40 and Table S8†). The oxidation potential shifted negatively when the core ring moieties became electron-rich (**1a**: 1.26 V, **1h**: 0.91, **1i**: 0.81 V, and **1j**: 0.58 V), while the reduction potential experienced minimal change. This indicates that the installation of electron-donating substituents on the pyrrole moiety effectively increases the HOMO energy levels, resulting in a narrowed HOMO–LUMO energy band gap. DFT calculations reveal that the calculated HOMOs for **1a**, **1i**, and **1j** are mostly distributed over the electron-rich pyrrole segments, with limited distribution over the BPh_2 and salicylhydrazide segments (Fig. S41†). In contrast, their LUMOs are distributed over the BOPSH core, indicating a classic ICT feature. Time-dependent DFT analysis assigns the main absorption peak to $S_0 \rightarrow S_1$ transitions with HOMO → LUMO contributions (Table S9†).

Chiroptical properties

The sp^3 hybridized boron atom (B1, Fig. 2a) bonds to four different atoms, inducing chirality in the fluorophore. These BOPSHs were crystallized as a 1 : 1 racemic mixture, with the axial phenyl moiety (on B1) pointing in opposite directions for enantiomers in each unit cell (Fig. S1–S7†). Using BOPSHs **1a**, **1i**, and **1j** as model compounds, we performed chiral separation and analysis using high-performance liquid chromatography (HPLC, Fig. S42–S50†). The optically resolved conformational enantiomers exhibited perfect mirror images of each other with opposite Cotton effects (Fig. 3 and S51–S53†). The chiral signals are ascribable to the distorted conformations of substituents on the pyrrole segment, as shown in the structures optimized by DFT. The absolute configurations of the respective enantiomers were elucidated by comparing experimental data with TD-DFT simulation results. Specifically, the Cotton effects for the main absorption band were found to be positive for the (*R*) configuration and negative for the (*S*) configuration (Fig. S54†). BOPSH **1a** exhibits $|g_{abs}|$ in dichloromethane (1.51×10^{-3}, Table S10†), while **1i** and **1j** exhibited similar CD characters with $|g_{abs}|$ values of 1.25×10^{-3} and 0.58×10^{-3}, respectively (Fig. S55† and Table 2). To understand why **1a** has relatively large dissymmetry factors, the dissymmetry factor (g_{abs}) is calculated using the formula: $g = 4\cos\theta|m|/|\mu|$, where θ is the angle between m and μ. The TD-DFT data listed in Table 2 reveals that **1a** has slightly smaller $|\mu|$ values but larger $\cos\theta$ values than those of respective BOPSH **1i**. The increased $\cos\theta$ values indicate the effective coupling of electric and magnetic

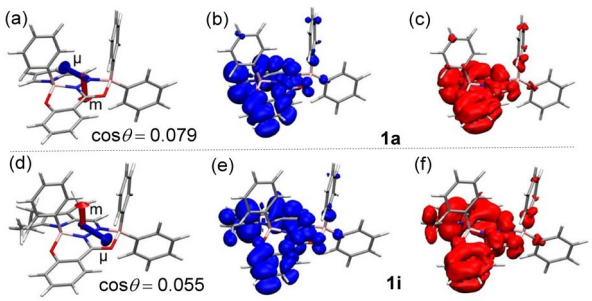

Fig. 4 Calculated magnetic (blue) and electronic (red) transition moment densities for BOPSHs **1a** (a)–(c) and **1i** (d)–(f) with an iso-value of 0.005.

Table 2 Chiroptical propertis of BOPSHs **1a** and **1i**

	g_{abs}[a] 10^{-3}	g_{lum}[b] 10^{-3}	g_{lum}[c] 10^{-3}	B_{CPL}[d] M^{-1} cm^{-1}	$\lvert\mu\rvert$[e] 10^{-18}	$\lvert m\rvert$[e] 10^{-20}	$\cos\theta$[e]	g_{calc}[f] 10^{-3}
1a	1.51	0.82	0.91	5.98	5.03	3.43	0.079	2.16
1i	1.25	0.50	1.00	3.93	5.84	3.34	0.055	1.26

[a] Corresponding g_{abs} of the (*R*)-configuration calculated as: g_{abs} = ellipticity/(32 980 × absorbance). [b] $g_{lum} = 2(I_L - I_R)/(I_L + I_R)$, dichloromethane. [c] g_{lum} obtained in powder solid states. [d] $B_{CPL} = \varepsilon \times \Phi_{PL} \times g_{lum}/2$. [e] Calculated at the CAM-B3LYP/6-311+G(d,p)/(IEFPCM, dichloromethane) level. $|\mu|$ unit: [esu cm], $|m|$ unit: [erg G^{-1}]. [f] Calculated using: $g = 4\cos\theta|m|/|\mu|$.

transition moments of **1a** (Fig. 4 and Table 2). These findings suggest that subtle electronic modifications can significantly impact the coupling of electric and magnetic transition moments.

The CPL spectra showed mirror–image relationships stemming from $S_1 \rightarrow S_0$ transitions with g_{lum} of up to 0.82×10^{-3} for (*R*)-**1a** and 1.39×10^{-3} for (*S*)-**1a** in dichloromethane, which are obviously higher than those outstanding bipyrrole-derived *tetra*-BF_2 flag-hinge chromophores reported by Ono.[24] The CPL maxima coincided with the emission maxima. Notably, the g_{lum} values for BOPSH **1a** in common organic solvents with different polarities and in solid states remained consistently around 10^{-3} (Fig. 3d–f, S56,† Table 2 and S11†). Additionally, the B_{CPL} values of **1a** and **1i** were determined to be 5.98 and 3.03 M^{-1} cm^{-1} using the formula: $B_{CPL} = \varepsilon \times \Phi_{PL} \times g_{lum}/2$, which is high for chiral BODIPY molecules. The B_{CPL} values, excellent photostability, and finely tuned emission properties suggest promising prospects for CPL-related biomedical and optoelectronic applications. Moreover, the CPL signals in solid states are stronger than those in solutions, with higher g_{lum} values of 0.91 $\times 10^{-3}$ (500 nm) for **1a** and 1.00 $\times 10^{-3}$ (530 nm) for **1i**, respectively. Furthermore, these BOPSHs are configurationally stable with a unique boron-stereogenic scaffold, and their enantiomers **1j** display g_{lum} values up to 9.40×10^{-3} (550 nm) and 4.52×10^{-3} (605 nm) in solid states. The increased chiroptical features may be attributed to the orderly or chirality-organized supramolecular array of chromophores within the crystalline lattice. To the best of our knowledge, these BOPSHs represent the first high-performance chiral DSE BODIPY analogues.

Electroluminescent performance

Motivated by the impressive chiral DSE characteristics and favourable HOMO/LUMO energy levels, we proceeded to study the electroluminescence (EL) behaviours of the enantiomers (R/S)-**1a** as chiral emitters within circularly polarized organic light-emitting diodes (CP-OLEDs).[25] The structure of the fabricated devices *via* vacuum deposition is as follows: ITO/MoO_3 (5 nm)/*m*CBP (25 nm)/EML (20 nm)/PO-T2T (5 nm)/TmPyPB (25 nm)/LiF (1 nm)/Al, in which indium tin oxide (ITO) serves as the transparent anode, 3,3′-di(9*H*-carbazol-9-yl)-1,1′-biphenyl (*m*CBP) functions as the hole-transporting layer, 2,4,6-tris[3-(diphenylphosphinyl)phenyl]-1,3,5-triazine (PO-T2T) acts as the exciton-blocking layer, 1,3,5-tri(*m*-pyrid-3-yl-phenyl)benzene (TmPyPB) serves as the electron-transporting layer, and LiF/Al acts as the cathode. The emitting layer (EML) is composed of 3 wt% (*R*)-**1a**: 48.5 wt% PO-T2T: 48.5 wt% *m*CBP for device A1, and 3 wt% (*S*)-**1a**: 48.5 wt% PO-T2T: 48.5 wt% *m*CBP for device A2, wherein PO-T2T and *m*CBP form an exciplex host for both chiral molecules. The device configuration diagram and the molecular structures of the functional layer are displayed in Fig. 5a and S57,† respectively. Notably, devices A1 and A2 can be turned on at low voltages of 3.1 and 3.0 V, which is due to the good injection and balanced transport of holes and electrons in the EML. Importantly, both devices radiate sky-blue light with EL peaks at 492 nm and maximum luminance (L_{max}) of 9559 and 9493 cd m^{-2} (Table S12†), respectively, demonstrating high brightness that is suitable for practical applications in solid-state displays (generally 100–1000 cd m^{-2}). The bright OLED emission of BOPSH **1a** can be attributed to the synergistic effect of dual boron anchoring and twisted molecular architecture.

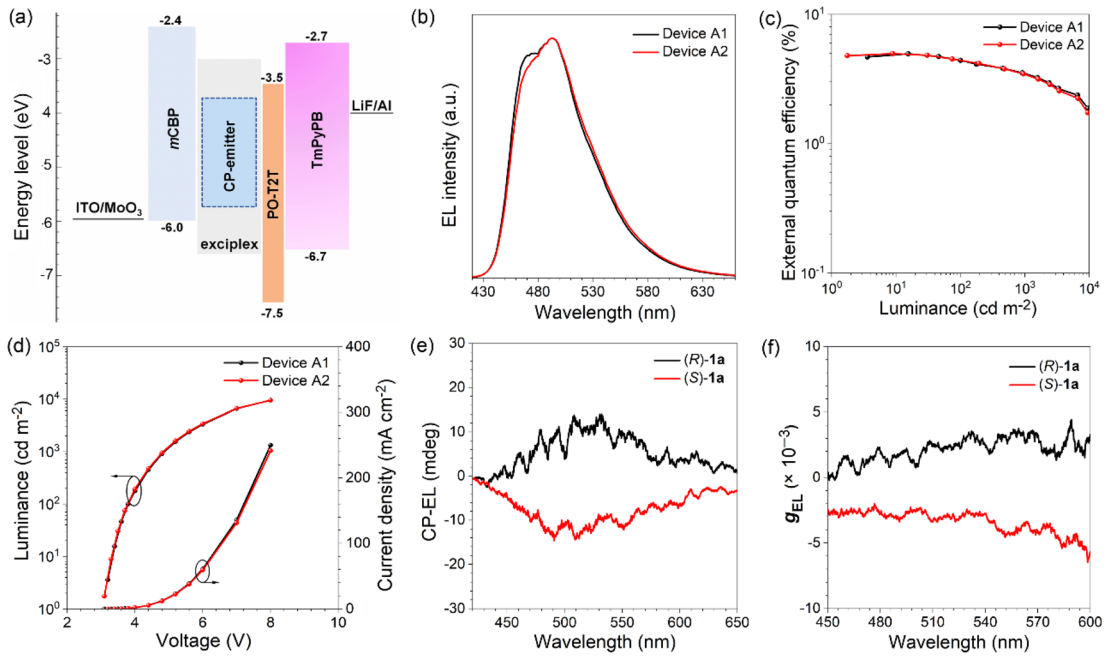

Fig. 5 (a) Configuration diagram of the fabricated devices. (b) EL spectra measured at 1000 cd m^{-2}, (c) external quantum efficiency curves with the change of luminance, and (d) luminance and current density curves with the change of voltage of devices A1 and A2. (e) CPEL spectra were collected under 5 V and (f) plots of g_{EL} *versus* CP-EL wavelength of devices A1 and A2.

More importantly, both devices attain excellent maximum external quantum efficiencies ($\eta_{ext,max}$) of 5.0% (Table S12†), which approaches the theoretical $\eta_{ext,max}$ limit for fluorescent molecules. This also indicates high exciton recombination efficiencies in both devices. Reliability tests (Tables S13 and S14†) on multiple devices confirm the consistent and reproducible performance of BOPSH-based OLEDs. Owing to their CPL nature, (*R*)-**1a** and (*S*)-**1a** exhibit good CP-EL properties, displaying mirror-image CP-EL spectra with good dissymmetry factor (g_{EL}) values of $+1.86 \times 10^{-3}$ and -3.07×10^{-3}, respectively (Fig. 5e and f). These results suggest that these new chiral molecules exhibit comparable g_{EL} to those of the recently developed CP-OLED devices[26] (Table S15†), and could serve as potential light-emitting materials for CP-OLEDs.

Conclusions

We present a facile approach to a dual-state-emissive boron stereogenic BOPSH fluorophore *via* a self-dispersing strategy. Our overall strategy involves the preparation of a suitable configurationally locked ligand featuring two independent boron coordination sites, followed by their subsequent *in situ* electrophilic aryl-boron substitutions to generate the target BOPSH fluorophore. The synthesis of these BOPSHs is achieved in a diversity-oriented one-pot fashion from commercial arylboronic acids, and easily accessible 2-formylpyrroles/indoles and salicylhydrazides. These BOPSHs show strong absorptions and DSE emissions in both solution (Φ approach to the unity) and solid states (Φ up to 89%), with a large Stokes shift, high photostability, and mechano-fluorescence. Additionally, they exhibit bright CPL with B_{CPL} values of up to 5.98 M^{-1} cm^{-1}. The fabricated CP-OLED devices achieved a high external quantum efficiency ($\eta_{ext,max} = 5.0\%$) with promising dissymmetry factors (g_{EL} up to 3.07×10^{-3}). These self-dispersing BOPSH fluorophores, along with their diversity-oriented one-pot synthesis, excellent DSE performance, and good CPL and CPEL properties, may provide a new perspective for constructing chiral DSE materials with diverse structures and functions.

Experimental

General synthetic procedure for boron-stereogenic BOPSHs 1

To a solution of pyrrole-2-carboxaldehyde derivative (PA, 1.0 mmol) and salicylhydrazide (167 mg, 1.1 mmol) in dried chlorobenzene (20 mL), several drops of glacial acetic acid (HOAc) were added slowly. The reaction mixture was refluxed in an oil bath at 105 °C for 6 h, and TLC was used to monitor the reaction. After the pyrrole-2-carboxaldehyde derivative disappeared on TLC, K_3PO_4 (690 mg, 3.0 mmol, 3 equiv) and the corresponding arylboronic acid (9.0 mmol, 9 equiv) were added into the mixture. The reaction was then stirred in a sealed tube at 140 °C overnight. After completion of the reaction, the mixture was poured into water (150 mL) and extracted with CH_2Cl_2 (3 × 60 mL). The organic layers were combined, dried over anhydrous Na_2SO_4, filtered, and evaporated under a vacuum. The crude product was purified by silica gel column chromatography and the yellow (or red) powders were obtained through recrystallization from dichloromethane and hexane.

Data availability

The ESI† includes all experimental details, including TD-DFT calculations, spectroscopic measurements, X-ray analysis, and the synthesis and characterization of all products reported in this study. NMR spectra of all products are also included.

Author contributions

C. Y., H. L., Z. Z., E. H., and L. J. supervised the work. C. Y. and C. C. designed the chemical synthetic route and conducted the experiments. Z. N. performed the calculations. Z. L conducted the electroluminescent measurements. C. Y. wrote the manuscript. All authors were involved in checking the data and have approved the final version of the manuscript.

Conflicts of interest

There are no conflicts to declare.

Acknowledgements

We thank the financial support provided by the National Natural Science Foundation of China (22271002, 22478005, and U23A20594), the Anhui Provincial Natural Science Foundation (2008085QB67, 2308085J14, and 2408085MB043), the Anhui Provincial University Scientific Research Project (2023AH050149), and the Interdisciplinary Research Project of Hangzhou Normal University (2024JCXK01) for supporting this work. We also thank Prof. Tianyu Yang from The Ninth Medical Center of the Chinese PLA General Hospital for generously sharing the CP-OLED data.

Notes and references

1 (*a*) L. E. MacKenzie and P. Stachelek, *Nat. Chem.*, 2021, **13**, 521–522; (*b*) G. Longhi, E. Castiglioni, J. Koshoubu, G. Mazzeo and S. Abbate, *Chirality*, 2016, **28**, 696–707; (*c*) W.-L. Zhao, M. Li, H.-Y. Lu and C.-F. Chen, *Chem. Commun.*, 2019, **55**, 13793–13803; (*d*) Y. Zhang, S. Yu, B. Han, Y. Zhou, X. Zhang, X. Gao and Z. Tang, *Matter*, 2022, **5**, 837–875.

2 (*a*) L. Arrico, L. Di Bari and F. Zinna, *Chem.–Eur. J.*, 2021, **27**, 2920–2934; (*b*) P. Stachelek, L. MacKenzie, D. Parker and R. Pal, *Nat. Commun.*, 2022, **13**, 553; (*c*) E. M. Sanchez-Carnerero, A. R. Agarrabeitia, F. Moreno, B. L. Maroto, G. Muller, M. J. Ortiz and S. de la Moya, *Chem.–Eur. J.*, 2015, **21**, 13488–13500.

3 (*a*) X. Yang, X. Gao, Y.-X. Zheng, H. Kuang, C.-F. Chen, M. Liu, P. Duan and Z. Tang, *CCS Chem.*, 2023, **5**, 2760–2789; (*b*) P. Zhao, W.-C. Guo, M. Li, H.-Y. Lu and C.-F. Chen, *Angew. Chem., Int. Ed.*, 2024, **63**, e202409020.

4 (*a*) Z.-L. Gong, X. Zhu, Z. Zhou, S.-W. Zhang, D. Yang, B. Zhao, Y.-P. Zhang, J. Deng, Y. Cheng, Y.-X. Zheng,

S.-Q. Zang, H. Kuang, P. Duan, M. Yuan, C.-F. Chen, Y. S. Zhao, Y.-W. Zhong, B. Z. Tang and M. Liu, *Sci. China Chem.*, 2021, **64**, 2060–2104; (*b*) Y. Deng, M. Wang, Y. Zhuang, S. Liu, W. Huang and Q. Zhao, *Light: Sci. Appl.*, 2021, **10**, 76.

5 F. Zinna and L. Di Bari, *Chirality*, 2015, **27**, 1–13.

6 X. Li, Y. Xie and Z. Li, *Adv. Photonics Res.*, 2021, **2**, 2000136.

7 (*a*) Y. Chen, *Mater. Today Chem.*, 2022, **23**, 100651; (*b*) T. Zhang, Y. Zhang, Z. He, T. Yang, X. Hu, T. Zhu, Y. Zhang, Y. Tang and J. Jiao, *Chem.–Asian J.*, 2024, **19**, e202400049; (*c*) Y. Deng, M. Wang, Y. Zhuang, S. Liu, W. Huang and Q. Zhao, *Light: Sci. Appl.*, 2021, **10**, 76.

8 (*a*) Y. Shen and C.-F. Chen, *Chem. Rev.*, 2012, **112**, 1463–1535; (*b*) W.-L. Zhao, M. Li, H.-Y. Lu and C.-F. Chen, *Chem. Commun.*, 2019, **55**, 13793–13803; (*c*) H. Lu and N. Kobayashi, *Chem. Rev.*, 2016, **116**, 6184–6261; (*d*) H. Lu, J. Mack, T. Nyokong, N. Kobayashi and Z. Shen, *Coord. Chem. Rev.*, 2016, **318**, 1–15.

9 (*a*) K.-K. Tan, W.-C. Guo, W.-L. Zhao, M. Li and C.-F. Chen, *Angew. Chem., Int. Ed.*, 2024, **136**, e202412283; (*b*) Y. Xu, P. Xu, D. Hu and Y. Ma, *Chem. Soc. Rev.*, 2021, **50**, 1030–1069; (*c*) S. Tang and L. Edman, *Top. Curr. Chem.*, 2016, **374**, 40; (*d*) J. Dong, L. Chen, Q. Feng and D.-T. Yang, *Angew. Chem., Int. Ed.*, 2024, **64**, e202417200; (*e*) K. Li, T.-B. Ren, S. Huan, L. Yuan and X.-B. Zhang, *J. Am. Chem. Soc.*, 2021, **143**, 21143–21160; (*f*) H.-W. Liu, L. Chen, C. Xu, Z. Li, H. Zhang, X.-B. Zhang and W. Tan, *Chem. Soc. Rev.*, 2018, **47**, 7140–7180.

10 (*a*) C. Liu, J.-C. Yang, J. W. Y. Lam, H.-T. Feng and B. Z. Tang, *Chem. Sci.*, 2022, **13**, 611; (*b*) M. Hu, H.-T. Feng, Y.-X. Yuan, Y.-S. Zheng and B. Zhong Tang, *Coord. Chem. Rev.*, 2020, **416**, 213329; (*c*) H.-T. Feng, C. Liu, Q. Li, H. Zhang, J. W. Y. Lam and B. Z. Tang, *ACS Mater. Lett.*, 2019, **1**, 192–202.

11 (*a*) L. A. Rodríguez-Cortés, F. J. Hernández, M. Rodríguez, R. A. Toscano, A. Jiménez-Sánchez, R. Crespo-Otero and B. Rodríguez-Molina, *Matter*, 2023, **6**, 1140–1159; (*b*) J. L. Belmonte-Vázquez, Y. A. Amador-Sánchez, L. A. Rodríguez-Cortés and B. Rodríguez-Molina, *Chem. Mater.*, 2021, **33**, 7160–7184.

12 (*a*) A. Loudet and K. Burgess, *Chem. Rev.*, 2007, **107**, 4891–4932; (*b*) G. Ulrich, R. Ziessel and A. Harriman, *Angew. Chem., Int. Ed.*, 2008, **47**, 1184–1201; (*c*) N. Boens, V. Leena and W. Dehaen, *Chem. Soc. Rev.*, 2012, **41**, 1130–1172; (*d*) H. Lu, J. Mack, Y. Yang and Z. Shen, *Chem. Soc. Rev.*, 2014, **43**, 4778–4823; (*e*) S. Wang, L. Gai, Y. Chen, X. Ji, H. Lu and Z. Guo, *Chem. Soc. Rev.*, 2024, **53**, 3976–4019; (*f*) T. Ozdemir, S. Atilgan, I. Kutuk, L. T. Yildirim, A. Tulek, M. Bayindir and E. U. Akkaya, *Org. Lett.*, 2009, **11**, 2105–2107; (*g*) H.-T. Feng, J.-B. Xiong, Y.-S. Zheng, B. Pan, C. Zhang, L. Wang and Y. Xie, *Chem. Mater.*, 2015, **27**, 7812–7819; (*h*) L. Gai, Y. Liu, Z. Zhou, H. Lu and Z. Guo, *Coord. Chem. Rev.*, 2023, **481**, 215041; (*i*) S. Wu, L. Gai, Z. Zhou and H. Lu, *Org. Chem. Front.*, 2022, **9**, 5989–6000.

13 (*a*) S. Wu, W. Zhang, C. Li, Z. Ni, W. Chen, L. Gai, J. Tian, Z. Guo and H. Lu, *Chem. Sci.*, 2024, **15**, 5973–5979; (*b*) M. Liu, S. Ma, M. She, J. Chen, Z. Wang, P. Liu, S. Zhang and J. Li, *Chin. Chem. Lett.*, 2019, **30**, 1815–1824; (*c*) J. Wang, C. Yu, E. Hao and L. Jiao, *Coord. Chem. Rev.*, 2022, **470**, 214709; (*d*) L. Gai, R. Zhang, X. Shi, Z. Ni, S. Wang, J. L. Zhang, H. Lu and Z. Guo, *Chem. Sci.*, 2023, **14**, 1434–1442.

14 (*a*) J. Jiménez, C. Díaz-Norambuena, S. Serrano, S. C. Ma, F. Moreno, B. L. Maroto, J. Bañuelos, G. Muller and S. de la Moya, *Chem. Commun.*, 2021, **57**, 5750–5753; (*b*) F. Zinna, T. Bruhn, C. A. Guido, J. Ahrens, M. Bröring, L. Di Bari and G. Pescitelli, *Chem.–Eur. J.*, 2016, **22**, 16089–16098; (*c*) R. B. Alnoman, S. Rihn, D. C. O'Connor, F. A. Black, B. Costello, P. G. Waddell, W. Clegg, R. D. Peacock, W. Herrebout, J. G. Knight and M. J. Hall, *Chem.–Eur. J.*, 2016, **22**, 93–96.

15 (*a*) E. M. Sánchez-Carnerero, F. Moreno, B. L. Maroto, A. R. Agarrabeitia, M. J. Ortiz, B. G. Vo, G. Muller and S. de la Moya, *J. Am. Chem. Soc.*, 2014, **136**, 3346–3349; (*b*) Y. Gobo, M. Yamamura, T. Nakamura and T. Nabeshima, *Org. Lett.*, 2016, **18**, 2719–2721; (*c*) A. Gossauer, F. Nydegger, T. Kiss, R. Sleziak and H. Stoeckli-Evans, *J. Am. Chem. Soc.*, 2004, **126**, 1772–1780; (*d*) G. Beer, C. Niederalt, S. Grimme and J. Daub, *Angew. Chem., Int. Ed.*, 2000, **39**, 3252–3255; (*e*) A. Haefele, C. Zedde, P. Retailleau, G. Ulrich and R. Ziessel, *Org. Lett.*, 2010, **12**, 1672–1675.

16 (*a*) M. Tsuji, S. Abuhadba, A. Chen, M. Ito, A. Makhijani, Y. Kuwahara, T. Esipova and T. Mani, *J. Phys. Chem. B*, 2023, **127**, 9781–9787; (*b*) Y. Gao, Z. Liu, S. Tian, Y. Min, X. Li, Y. Chen, X. Hong, W. Zhang and L. Wang, *Angew. Chem., Int. Ed.*, 2024, e202418888.

17 (*a*) Y. Xu, Z. Ni, Y. Xiao, Z. Chen, S. Wang, L. Gai, Y.-X. Zheng, Z. Shen, H. Lu and Z. Guo, *Angew. Chem., Int. Ed.*, 2023, **62**, e202218023; (*b*) J. Full, S. P. Panchal, J. Götz, A.-M. Krause and A. Nowak-Król, *Angew. Chem., Int. Ed.*, 2021, **60**, 4350–4357; (*c*) C. Maeda, K. Nagahata, T. Shirakawa and T. Ema, *Angew. Chem., Int. Ed.*, 2020, **59**, 7813–7817; (*d*) C. Maeda, K. Nagahata, T. Shirakawa and T. Ema, *Angew. Chem., Int. Ed.*, 2020, **59**, 7813–7817; (*e*) T. Bruhn, G. Pescitelli, S. Jurinovich, A. Schaumlöffel, F. Witterauf, J. Ahrens, M. Bröring and G. Bringmann, *Angew. Chem., Int. Ed.*, 2014, **53**, 14592–14595; (*f*) Z. Chen, Z. Ni, X. Y. Chen, Y. Xu, C. Yu, S. Wang, X. Y. Wang and H. Lu, *Aggregate*, 2024, e498.

18 (*a*) A. Abdou-Mohamed, C. Aupic, C. Fournet, J.-L. Parrain, G. Chouraqui and O. Chuzel, *Angew. Chem., Int. Ed.*, 2024, e202418888; (*b*) X. Li, G. Zhang and Q. Song, *Chem. Commun.*, 2023, **59**, 3812–3820; (*c*) M. Braun, *Eur. J. Org Chem.*, 2024, **27**, e202400052.

19 (*a*) B. Zu, Y. Guo and C. He, *J. Am. Chem. Soc.*, 2021, **143**, 16302–16310; (*b*) L.-Y. Wang, Z.-F. Liu, K.-X. Teng, L.-Y. Niu and Q.-Z. Yang, *Chem. Commun.*, 2022, **58**, 3807–3810; (*c*) B. Zu, Y. Guo, L.-Q. Ren, Y. Li and C. He, *Nat. Synth.*, 2023, **2**, 564; (*d*) L.-Q. Ren, B. Zhan, J. Zhao, Y. Guo, B. Zu, Y. Li and C. He, *Nat. Chem.*, 2024, **17**, 83–91; (*e*) G. Zhang, Z. Zhang, M. Hou, X. Cai, K. Yang, P. Yu and Q. Song, *Nat. Commun.*, 2022, **13**, 2624; (*f*) G. Zhang,

X. Cai, J. Jia, B. Feng, K. Yang and Q. Song, *ACS Catal.*, 2023, **13**, 9502–9508.
20 (*a*) M. Wang and C.-H. Zhao, *Chem. Rec.*, 2022, **22**, e202100199; (*b*) C.-H. Chen and W.-H. Zheng, *Org. Lett.*, 2021, **23**, 5554–5558.
21 P. v. R. Schleyer, C. Maerker, A. Dransfeld, H. Jiao and N. J. R. van E. Hommes, *J. Am. Chem. Soc.*, 1996, **118**, 6317–6318.
22 H. Cao, Y. Gao, B. Wu, J. Zhang, L. Wang, P. Wei, L. Liu, H. Zou, H. Zhou, Z. Zheng and B. Z. Tang, *Angew. Chem., Int. Ed.*, 2024, **34**, 2315692.
23 S. Choi, J. Bouffard and Y. Kim, *Chem. Sci.*, 2014, **5**, 751–755.
24 L. Cui, H. Shinjo, T. Ichiki, K. Deyama, T. Harada, K. Ishibashi, T. Ehara, K. Miyata, K. Onda, Y. Hisaeda and T. Ono, *Angew. Chem., Int. Ed.*, 2022, **61**, e202204358.
25 L. Xu, H. Liu, X. Peng, P. Shen, B. Z. Tang and Z. Zhao, *Angew. Chem., Int. Ed.*, 2023, **62**, e202300492.
26 R. Zhang, J. Gao, N. Li, C. Gao, C. Zhang, H. Wang, F. Sun and T. Yang, *Small*, 2025, 2409541.